Trajectory of a test particle around a slowly rotating relativistic star emitting isotropic radiation

Jae Sok Oh*
Department of Physics and Astronomy, FPRD, Seoul National University, Seoul 151-742, Korea

Hongsu Kim†
Korea Astronomy and Space Science Institute, Daejeon 305-348, Korea

Hyung Mok Lee‡
Department of Physics and Astronomy, FPRD, Seoul National University, Seoul 151-742, Korea
(Received 26 October 2009; published 1 April 2010)

We explored the motion of test particles near slowly rotating relativistic star having a uniform luminosity. In order to derive the test particle's equations of motion, we made use of the radiation stress-energy tensor first constructed by Miller and Lamb [3]. From the particle's trajectory obtained through the numerical integration of the equations of motion, it is found that for sufficiently high luminosity, ''suspension orbit'' exists, where the test particle hovers around at uniform angular velocity in the same direction as the star's spin. Interestingly, it turned out that the radial position of the suspension orbit was determined by the luminosity and the angular momentum of the star alone and was independent of the initial positions and the specific angular momentum of the particle. Also found is that there exist not only the radiation drag but also ''radiation counter drag,'' which depends on the stellar radius and the angular momentum, and it is this radiation counterdrag that makes the test particle in the suspension orbit hover around at a uniform angular velocity that is greater than that induced by the Lense-Thirring effect (i.e., general relativistic dragging of inertial frame).

DOI: 10.1103/PhysRevD.81.084005 PACS numbers: 04.20.−q, 95.30.Gv, 97.60.Jd

I. INTRODUCTION

Astrophysical accretion flow onto massive or compact stars is one of the major concerns in astronomy and astrophysics. In the present work, we explore the ground work for the full understanding of the accretion flow onto highly luminous slowly rotating relativistic stars. In the current treatment of the accretion process, the effect of radiation pressure on the inflow has not been fully addressed. Therefore, in the present work, we attempt to include systematically the role of the radiation pressure in the accretion process. To this end, we explore the effect of the radiation pressure on the motion of a single test particle. Eventually we hope that this elementary study of ours will be extended to the case of actual accretion flow, which can be thought of as consisting of large number of constituent single particles.

We now begin with the summary of the present status of the research in the literature along this line. In their pioneering work, Abramowicz, Ellis, and Lanza [1] demonstrated that radiation from the highly luminous nonrotating spherical massive star generates a ''critical point'' above the stellar surface, but they limited the motion of the particles to one-dimensional radial direction alone and did not deal with the case of rotating central stars emitting isotropic radiation. Later on, Miller and Lamb [2] extended one-dimensional motion to a two-dimensional one and pointed out that the trajectory of the particle is significantly affected by the radiation from the nonrotating star if the luminosity of the star is greater than $\sim 1\%$ of the Eddington luminosity. They, however, confined themselves to the spherical symmetric spacetime describing the nonrotation of the central star. Some time later, they considered [3] the effects of slow rotation of the central star and constructed the radiation stress-energy tensor describing the radiation field from the slowly rotating central star. They, however, failed to notice the emergence of critical radius (which corresponds to the critical point reported in Abramowicz *et al.* [1]) as they considered the setup in which the luminosity is well below Eddington's critical value.

In the present work, in order to understand the effects of the radiation pressure on the accretion onto the highly luminous rotating relativistic stars in a rigorous and complete manner, we employ the radiation stress-energy tensor that is given by Miller and Lamb [3] as an elaboration on that given originally by Abramowicz *et al.* [1] to describe the radiation emitted from the slowly rotating central stars, and derive the equation of motion.

By integrating numerically the equations of motion, we realized that there exists the suspension orbit (where the test particle hovers around the central star) that corresponds to the ''critical point'' in [1]. And it turns out that the radial position of this suspension orbit depends on the luminosity and the angular momentum of the central star alone, and does not depend on the initial position and the initial angular momentum of the test particles.

*ojs@astro.snu.ac.kr
†hongsu@kasi.re.kr
‡hmlee@astro.snu.ac.kr

In addition, it is realized that the test particle in the suspension orbit has uniform azimuthal velocity in the same direction as the star's spin motion. It is interesting to note that the uniform azimuthal velocity of the test particle at the suspension orbit is greater than that due to the Lense-Thirring effect.

In Sec. II, we provide the derivation of the equations of motion from the known radiation stress-energy tensor and discuss the usual radiation drag terms and the newly discovered radiation counter-drag terms. In Sec. III, we present the results of the numerical integrations showing the emergence of the suspension orbit. In Sec. IV, we analyze the motion of the particle in the suspension orbit, and finally, in Sec. V, we end with a discussion of our results.

II. EQUATIONS OF MOTION

To derive the equations of motion that govern the trajectory of the test particles in the presence of radiation from the slowly rotating relativistic star, we assume that the radiation source emits isotropically the radiation from the whole stellar surface, and we employ the following metric obtained from the Kerr black hole metric ([4]) by retaining its terms to the first order in the Kerr parameter a to represent the spacetime exterior to the slowly rotating star,

$$\begin{aligned} ds^2 &= g_{\mu\nu}dx^\mu dx^\nu \\ &= -(1-2M/r)dt^2 + (1-2M/r)^{-1}dr^2 + r^2d\theta^2 \\ &\quad + r^2\sin^2\theta(d\phi^2 - 2\omega d\phi dt), \end{aligned} \tag{1}$$

where $\omega = 2J/r^3$ is the Lense-Thirring angular velocity [5] arising due to the frame-dragging effect of a stationary axisymmetric spacetime, which can be identified with the orbital angular velocity of the LNRF (locally non-rotating frame); see [6,7]. M and J are the gravitational mass and angular momentum of the star, respectively. We work in the geometric units, where $G = c = 1$ (G is the gravitational constant and c is the speed of light). Following Miller and Lamb [3], we introduce a dimensionless angular momentum $j \equiv cJ/(GM^2)$ and dimensionless velocity $v \equiv \langle v^{\hat{\phi}}\rangle/c$ as a convenient measure of the rotation rate of the star and the rotation rate of the radiation source, respectively, where $\langle v^{\hat{\phi}}\rangle$ is the appropriate average (see [3]) of $v^{\hat{\phi}}$ (azimuthal linear velocity) over the emitting surface visible from the test particle. The hat denotes the physical quantity measured in the LNRF. In this paper "slow rotation" means $j \ll 1$ and $v \ll 1$, and we keep terms that are only first order in j and v. For a neutron star with radius $R \approx 10$ km, mass $M \approx 1.4M_\odot$, and spin frequency $\nu_s \approx 600$ Hz (i.e., a millisecond pulsar), the dimensionless angular momentum j is approximately 0.2.

The equations of motion (which actually is the geodesic equation) are given by

$$a^\alpha = \frac{f^\alpha}{m}, \tag{2}$$

where f^α denotes a radiation force exerted by the radiation (or luminosity) on the test particle, m is the rest mass of the particle, and

$$a^\alpha = \frac{dU^\alpha}{d\tau} + \Gamma^\alpha_{\mu\nu}U^\mu U^\nu \tag{3}$$

is the acceleration, with U^α being the four-velocity of the particle, $\Gamma^\alpha_{\mu\nu} = \frac{1}{2}g^{\alpha\beta}(g_{\beta\mu,\nu} + g_{\beta\nu,\mu} - g_{\mu\nu,\beta})$ being the Affine connection, with a comma (,) denoting partial derivatives.

For the sake of computational convenience, like in [3], we assumed that the radiation scatters off the test particles and the momentum-transfer cross section σ of the test particle is independent of energy (frequency) and direction of the radiation. Hence, the radiation force f^α due to scattering of the radiation is proportional to and in the direction of the radiation flux in the comoving frame (particle's rest frame), and is given by (see [8])

$$f^\alpha = \sigma F^\alpha, \tag{4}$$

where F^α is the quantity obtained by transforming the radiation energy flux $T^{\hat{i}\hat{0}}_{co}$ measured in the comoving frame using the orthonormal tetrad $\tilde{e}^\alpha_{\hat{i}}$ associated with the particle's rest frame as follows:

$$F^\alpha = \tilde{e}^\alpha_{\hat{i}}T^{\hat{i}\hat{0}}_{co} = -h^\alpha_\beta T^{\beta\sigma}U_\sigma, \tag{5}$$

where $h^\alpha_\beta = \delta^\alpha_\beta + U^\alpha U_\beta$ is the projection tensor that projects onto each spacelike hypersurface, and $T^{\beta\sigma}$ is the radiation stress-energy tensor in first order (in j) Boyer-Lindquist coordinates (see [3]) (for $j \neq 0$).

According to [3], the components of the radiation stress-energy tensor $T^{\hat{\alpha}\hat{\beta}}$ as measured in LNRF are given by

$$\begin{aligned} T^{\hat{t}\hat{t}} &\approx 2\pi I_0(r)(1-\cos\alpha_0), \\ T^{\hat{t}\hat{r}} &\approx \pi I_0(r)\sin^2\alpha_0, \\ T^{\hat{t}\hat{\phi}} &\approx \frac{\pi}{3}I_0(r)\mathcal{J}(r)(\cos^3\alpha_0 - 3\cos\alpha_0 + 2), \\ T^{\hat{r}\hat{r}} &\approx \frac{2\pi}{3}I_0(r)(1-\cos^3\alpha_0), \\ T^{\hat{r}\hat{\phi}} &\approx \frac{\pi}{4}I_0(r)\mathcal{J}(r)\sin^4\alpha_0, \\ T^{\hat{\theta}\hat{\theta}} &\approx \frac{\pi}{3}I_0(r)(\cos^3\alpha_0 - 3\cos\alpha_0 + 2), \\ T^{\hat{\phi}\hat{\phi}} &\approx \frac{\pi}{3}I_0(r)(\cos^3\alpha_0 - 3\cos\alpha_0 + 2), \end{aligned} \tag{6}$$

where the subscript 0 denotes the quantity for the case of nonrotating star, α_0 is an apparent viewing angle of the star

seen by a locally static observer in Schwarzschild spacetime and is given by $\sin\alpha_0 = (\frac{R}{r})(\frac{1-2M/r}{1-2M/R})^{1/2}$ (see [1]) for the radius of the star $R \geq 3M$, and $I_0(r)$ is the frequency-integrated specific intensity at the radial position r and is given by (see Appendix A in [3])

$$I_0(r) = \frac{(1-2M/R)}{(1-2M/r)^2}\frac{mM}{\pi\sigma R^2}\left(\frac{L^\infty}{L^\infty_{\rm Edd}}\right), \tag{7}$$

where the Eddington luminosity $L^\infty_{\rm Edd} \equiv 4\pi mM/\sigma$ is the luminosity of a spherically symmetric source such that at infinity the outward radiation force balances the inward gravity (see [8]), and L^∞ is the luminosity of the star as measured by an observer at infinity, and $\mathcal{J}(r)$ is given by

$$\mathcal{J}(r) = 8j\left(\frac{r}{M}\right)\left(\frac{M^3}{R^3} - \frac{M^3}{r^3}\right) + 4v\left(\frac{r}{R}\right)(1-2M/R)^{1/2}. \tag{8}$$

By transforming the above radiation stress-energy tensor $T^{\hat\mu\,\hat\nu}$ to the LNRF using tetrad $e^\alpha_{\hat\mu}$ (which is given below) associated with the LNRF, the radiation stress-energy tensor $T^{\alpha\beta}$ in the first-order Boyer-Lindquist coordinates (see [3]) is obtained as

$$T^{\alpha\beta} = e^\alpha_{\hat\mu} e^\beta_{\hat\nu} T^{\hat\mu\,\hat\nu}, \tag{9}$$

where the tetrad associated with the LNRF are

$$e^{\hat 0} = (1-2M/r)^{1/2}dt, \qquad e^{\hat 1} = (1-2M/r)^{-1/2}dr,$$
$$e^{\hat 2} = rd\theta, \qquad e^{\hat 3} = -2j\frac{M^2}{r^2}\sin\theta + r\sin\theta d\phi. \tag{10}$$

We now focus our attention on the orbits confined to the equatorial plane ($\theta = \frac{\pi}{2}$, $U_\theta = 0$). The decomposition into each component of the equations of motion (5) in tensor form is given in the Appendix. It should also be noted that as the radiation stress-energy tensor [Eq. (6)] first constructed by Miller and Lamb [3] is valid up to $j = 0.20$, and the equations of motion derived from it are also valid within the above ranges.

Since the background spacetime of Eq. (1) has a rotational isometry, the Killing theorem states that there exists a rotational Killing field $\eta^\mu = \delta^\mu_\phi$ such that the test particle's specific angular momentum $l = g_{\mu\nu}\eta^\mu U^\nu = g_{\mu\nu}\delta^\mu_\phi U^\nu = g_{\phi\nu}U^\nu = U_\phi$ is conserved. Therefore, the azimuthal component [Eq. (A3)] of the equations of motion in the Appendix governs the time evolution of the test particle's specific angular momentum and can be rewritten as

$$\begin{aligned}\frac{dU_\phi}{d\tau} = &-\frac{L}{3}\frac{f(r)}{(1-2M/r)}\Big[A(\alpha_0)U_t^2 + \left(1-\frac{2M}{r}\right)^2 \\ &\times(\cos\alpha_0\sin^2\alpha_0)U_r^2\Big]U_\phi - \frac{L}{3}\frac{f(r)}{(1-2M/r)} \\ &\times\Big[4j\left(\frac{M^2}{r^3}\right)A(\alpha_0)U_\phi^2 + r\mathcal{J}(r)B(\alpha_0) \\ &+\left(\frac{2}{r}\right)\mathcal{J}(r)B(\alpha_0)U_\phi^2\Big]U_t \\ &- Lf(r)\Big[(2\sin^2\alpha_0)U_tU_\phi + 4j\left(\frac{M^2}{r^3}\right)(\sin^2\alpha_0)U_\phi^2\Big]U_r \\ &- Lf(r)\Big[\left(\frac{r}{4}+\frac{1}{2r}U_\phi^2\right)\Big]\mathcal{J}(r)(\sin^4\alpha_0)U_r,\end{aligned} \tag{11}$$

where $A(\alpha_0) = \cos^3\alpha_0 - 9\cos\alpha_0 + 8$, $B(\alpha_0) = \cos^3\alpha_0 - 3\cos\alpha_0 + 2$, $L \equiv (\frac{L^\infty}{L^\infty_{\rm Edd}})$ is the luminosity parameter, and $f(r) = \frac{M}{R^2}\frac{(1-2M/R)}{(1-2M/r)^2}$.

We are now ready to envisage the features of the solution to the azimuthal component of the equation of motion given in Eq. (11). Obviously, however, the analytic solution to this coupled nonlinear ordinary differential Eq. (11) is not readily available. Therefore, we shall look for its numerical solution in the next section. However, even before that we can read off the essential features of the solution. To this end, we will interpret this azimuthal component of the equation of motion as the equation that determines the time evolution of the test particle's specific angular momentum as $U_\phi = l$. To summarize, this azimuthal component of equation of motion breaks into three parts: the first part is line one of Eq. (11) and the two terms in this line are responsible for the radiation drag, that is, the well-known Poynting-Robertson effect since it is manifest that the overall sign of this line is negative definite, and these two terms are linearly proportional to the test particle's specific angular momentum U_ϕ and the star's luminosity. The second part is line two of Eq. (11) and the three terms in this line are responsible for the radiation counter drag that has the effect opposite to the Poynting-Robertson effect since it is obvious that the overall sign of line two is positive definite. The third part consists of line three and line four of Eq. (11), and terms with opposite signs can be regarded as being responsible for, say, radiation drag for one sign and radiation counter drag for the other. Now, in what follows, let us be more specific about the nature of each term in these lines. For instance, the first term in line two is due to the Lense-Thirring effect, that is, the dragging of inertial frame and the second and third terms in line two are due to the spin of the central star. Next, the second term in line three is due to the Lense-Thirring effect and the two terms in line four are due to the spin of the central star.

It is interesting to note that although the radiation drag or the Poynting-Robertson effect has been long known, the nature of this effect has not been unveiled manifestly thus far. In Eq. (11) above, however, we were successful in

quantifying this Poynting-Robertson effect by explicitly identifying the terms in line one that are responsible for the effect. In other words, by examining the equation of motion of a test particle placed in the background of a luminous relativistic spinning star, we demonstrated manifestly that the Poynting-Robertson effect actually takes place. Interestingly, however, this is not the end of the story. Remarkably, in the test particle's equation of motion, there are also terms that appear to be responsible for the effect just opposite to the Poynting-Robertson effect, that is, terms in line two and some more terms in lines three and four. This last point appears to imply that particularly for the luminous relativistic spinning star, the new effect just opposite to the Poynting-Robertson effect, which will be coined henceforth as the ''radiation counter drag,'' takes place as well. To the best of our knowledge, the counter-drag effect of this sort has never been reported in the literature so far. Therefore, in the following sections, we will solve the test particle's equation of motion numerically to construct and investigate quantitative solutions that will support our analysis of the features of the solutions stated above. What is more, based on both this numerical analysis and analytical approach, we will report on the emergence of the suspension orbit (which turns out to be the extension of the critical point pointed out in earlier study [1] in the absence of star's rotation).

III. NUMERICAL INTEGRATION

In this subsection, we shall present the numerical solution to the equations of motion derived in Sec. II. We begin with a brief description of our treatment of this numerical analysis. Using the equations of motion derived in Sec. II, we have followed the trajectory of the particle in the presence of radiation from the slowly rotating star. We confine the motion of the particle onto the equatorial plane so that the polar angle component of the velocity U_θ is set to be zero ($U_\theta = 0$). We assume that the star has uniform density, so the angular velocity of the star and the angular velocity of the LNRF at the stellar surface are given, respectively, by $\Omega = \frac{5}{2} j(\frac{M}{R^2})$ and $\omega = 2j(\frac{M^2}{R^3})$. Thus, the average azimuthal velocity $v^{\hat{\phi}}$ of the radiation source as measured by an observer in the LNRF is calculated to be

$$v = \frac{1}{\pi} j\left(\frac{M^2}{R^2}\right)\left(1 - \frac{2M}{R}\right)^{-1/2}\left[5\left(\frac{R}{M}\right) - 4\right].$$

Figure 1 shows the trajectories of the particles starting at the position of $r = 6M$, where the particles have three azimuthal velocities of 0.10 (dotted curve), 0.25 (dashed curve), and 0.30 (dashed-dotted curve), respectively. Initial radial velocities of all the particles are equal to zero, and the luminosity parameter of the star with $R = 4M$ is $L = 0.75$. The solid line with a radius of $4M$ denotes the stellar surface, and the long dashed circle is the virtual circular orbit with radius of $r = 6M$ (i.e., ISCO; innermost stable circular orbit). The starting point of all the particles are the same as $(6M, 0)$ in Cartesian coordinates (x, y). The rotation of the star is counterclockwise. Hence, the particles start at counterclockwise rotational motion.

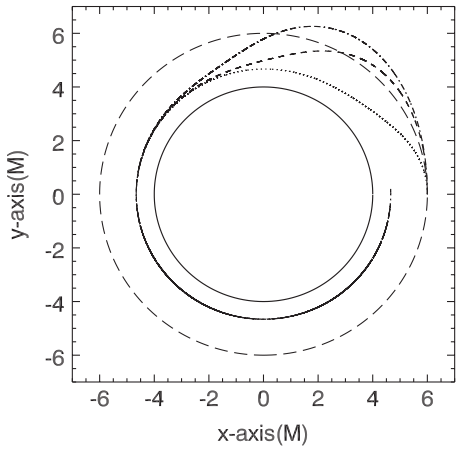

FIG. 1. shows the trajectories of the particles having three azimuthal velocities of 0.10 (dotted curve), 0.25 (dashed curve), and 0.30 (dashed-dotted curve), respectively, when they initially corotate with the star (which is rotating counterclockwise all the way) having angular momentum $j = 0.1$.

As can be seen in Fig. 1, although the three particles start out in different azimuthal velocities, they end up being along the same circular orbit, which we henceforth shall refer to the suspension orbit. It turns out that this suspension orbit lies in between the stellar surface (i.e., $r = 4M$) and the ISCO (i.e., $r = 6M$). According to the numerical analysis, its radius is given by $r = 4.66M$.

Figure 2 shows the radial velocities of the particles in Fig. 1 inflowing toward the stellar surface from $r = 6M$ as a function of the radius. Numerical integration demonstrates that the radial velocities of the particles at the suspension orbit vanish, and the time rate of change of

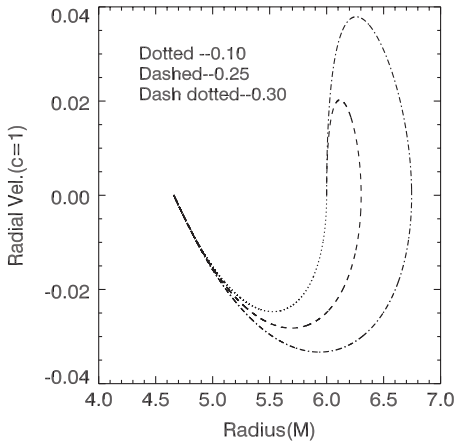

FIG. 2. shows locally measured radial velocities as functions of radius for particles in Fig. 1 inflowing from $r = 6M$ toward the suspension orbit.

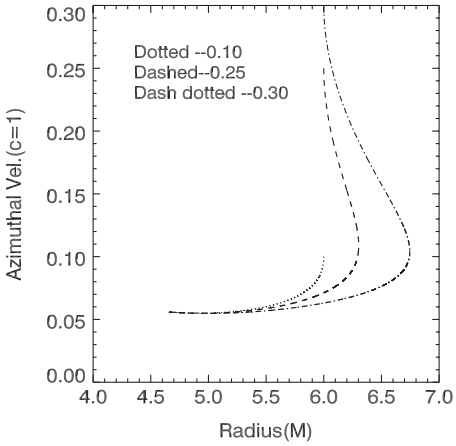

FIG. 3. shows locally measured azimuthal velocities as functions of radius for particles in Fig. 1 inflowing from $r = 6M$ toward the suspension orbit.

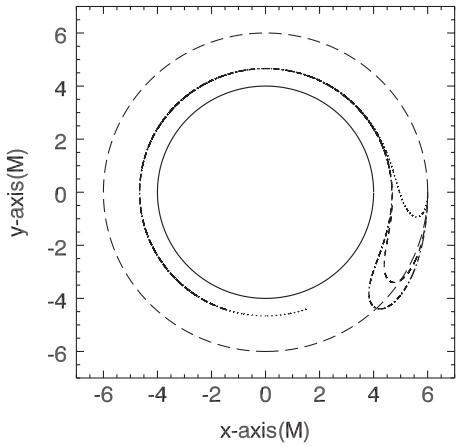

FIG. 4. shows the trajectories of the particles having three azimuthal velocities of -0.10 (dotted curve), -0.25 (dashed curve), and -0.30 (dashed-dotted curve), respectively, when they initially counter rotate with the star (which is rotating counterclockwise all the way) having angular momentum $j = 0.1$ but end up being corotating with the star mainly due to the radiation counter drag.

the radial velocities is also equal to zero, i.e., $U_r = 0$ and $\frac{dU_r}{d\tau} = 0$ at the suspension orbit.

Figure 3 shows the azimuthal velocities of the particles in Fig. 1 as a function of the radius, and there we can figure out that the azimuthal velocities $v^{\tilde{\phi}}$ of the particles at the suspension orbit as measured by a locally static observer are all equal to $v^{\tilde{\phi}} \simeq 0.056$ in units of c (the speed of light), and the time rate of change of the azimuthal velocities is equal to zero, i.e., $U_\phi =$ constant and $\frac{dU_\phi}{d\tau} = 0$ at the suspension orbit. These indicate that the particles orbit at constant speed there. Remarkably, essentially the same is true for the case where the central star is not rotating. This point appears to indicate that the emergence of both the critical point for the case of the nonrotating central star and the suspension orbit for the present case of the rotating central star are indeed a generic feature that a high luminosity relativistic star exhibits.

Thus far in Figs. 1–3, we have studied the case where the central star and the test particles "corotate" all the way. Next, we move on to the other case where they counter-rotate initially but end up corotating eventually and here, the rotation of the star is counterclockwise all the way. The result is given in Figs. 4–6.

To summarize, in Figs. 1–3, we have studied the case where the central star and the test particles corotate all the way. In Figs. 4–6, however, we have studied the other case where they counter-rotate initially but end up corotating eventually. Namely, regardless of initial conditions, i.e., whether they are initially corotating or counterrotating, the system reaches the same final equilibrium state where the test particles end up corotating with the central star. This result indeed is very interesting and curious particularly for the case when the central luminous star is spinning since the eventual fate of the test particles is the corotation with the central star at the suspension orbit. Therefore, we need a careful understanding of the underlying physics, and our interpretation is based upon the geodesic equation of the test particles at the suspension orbit given in Eq. (13) below, and it can be described as follows.

First, the first line term in Eq. (13) plays the role of radiation drag because its overall sign is negative definite due to $U_t < 0$ and is proportional to the test particle's specific angular momentum U_ϕ. Note that the radiation drag of the first line term works on the test particle regardless of the spin of the central star.

Secondly, fourth line terms, on the other hand, play the role of radiation counter drag because its overall sign is positive definite and is proportional to the central star's angular momentum j. Note that the radiation counter drag of these fourth line terms work on the test particle regardless of the test particle's specific angular momentum U_ϕ.

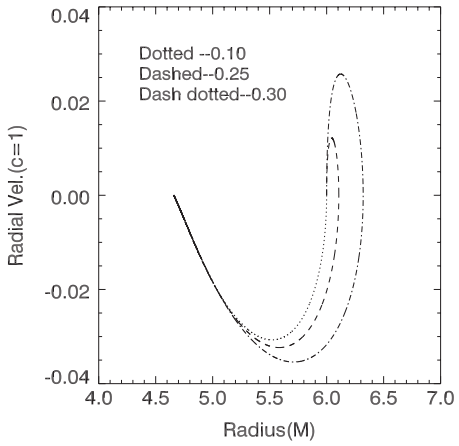

FIG. 5. shows locally measured radial velocities as functions of radius for particles in Fig. 4 inflowing from $r = 6M$ toward the suspension orbit.

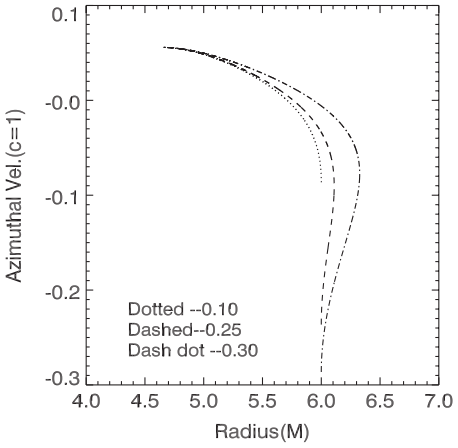

FIG. 6. shows locally measured azimuthal velocities as functions of radius for particles in Fig. 4 inflowing from $r = 6M$ toward the suspension orbit.

Indeed, the radiation drag term in the first line of Eq. (13), which represent the Poynting-Robertson effect, is well known, and it is generic as it is independent of the central star's angular momentum. The radiation counter-drag terms in the fourth line have been neglected in our conventional understanding of the Poynting-Robertson effect and hence is rather unfamiliar. Besides, it is not so generic as it appears only in the presence of the central star's angular momentum. Therefore, unlike the case where the central luminous star is nonrotating, for the case at hand where the central star is spinning, not only the radiation drag term in the first line but the radiation counter-drag terms in the fourth line operate as well and indeed they would affect the motion of the test particle on equal footing to determine its trajectory. Interestingly enough, our numerical study above exhibits that once the test particle arrives at the suspension orbit, it never comes to a complete stop. Rather, it keeps corotating with the central luminous spinning star, and this is the new discovery of the present work, which has not been realized in the previous literature addressing similarly related issues.

As can be noticed from the numerical integration, the radiation from the slowly rotating star makes the test particles hover around the star with uniform azimuthal velocity regardless of the initial position, and the initial angular momentum of the particle and the particle's motion in the suspension orbit is characterized by the following conditions:

$$U_r = 0 \qquad U_\phi = \text{constant} \qquad \frac{dU_r}{d\tau} = \frac{dU_\phi}{d\tau} = 0.$$

IV. EXAMINATION OF THE MOTION IN THE SUSPENSION ORBIT

In order to understand the nature of ''forces'' exerted on the particle hovering around the suspension orbit, let us examine the equations of motion using the conditions mentioned above in Sec. III and then determine the coordinate radius of the suspension orbit and the azimuthal velocity of the particle as measured by the locally static observer.

By inserting $U_r = 0$ and $\frac{dU_\phi}{d\tau} = 0$ of the conditions for the suspension orbit into the ϕ component [Eq. (11)] of the equations of motion, we obtain the following:

$$\left[4j\frac{M^2}{r^2}A(\alpha_0) + 2\mathcal{J}(r)B(\alpha_0)\right]U_\phi^2 + rA(\alpha_0)U_\phi U_t + r^2\mathcal{J}(r)B(\alpha_0) = 0, \tag{12}$$

where the luminosity parameter L as a common factor is omitted. Then, plugging $\mathcal{J}(r)$ in Eq. (8) into the above Eq. (12) gives, after some manipulation,

$$\begin{aligned} 0 &= \frac{dU_\phi}{d\tau} \\ &= A(\alpha_0)U_t U_\phi + 4j\left(\frac{M^2}{r^3}\right)[A(\alpha_0) - 4B(\alpha_0)]U_\phi^2 \\ &\quad + 8B(\alpha_0)\left[2j\left(\frac{M^2}{R^3}\right) + v\left(\frac{1}{R}\right)(1 - 2M/R)^{1/2}\right]U_\phi^2 \\ &\quad + 8j\left(\frac{r^2}{R^3} - \frac{1}{r}\right)M^2B(\alpha_0) \\ &\quad + 4v\left(\frac{r^2}{R}\right)(1 - 2M/R)^{1/2}B(\alpha_0). \end{aligned} \tag{13}$$

First, terms in line one in Eq. (13) play the role of radiation drag because its overall sign is negative definite due to $U_t < 0$ and is proportional to the test particle's specific angular momentum U_ϕ. Therefore, the radiation drag terms in line one work on the test particle having the azimuthal velocity U_ϕ regardless of the spin of the central star. Second, as $[A(\alpha_0) - 4B(\alpha_0)]$ of line two in Eq. (13) has positive value for $\alpha_0 \neq 0$, the overall sign of line two is positive definite, thus this line serves as the radiation counter drag that speeds up the azimuthal motion. It should also be noted that this line two is proportional to the Lense-Thirring angular velocity $\omega = 2j(\frac{M^2}{r^2})$ and the test particle's specific angular momentum square U_ϕ^2, thus the radiation counter drag of line two is due to the Lense-Thirring effect arising from the rotation of the central star. Unfortunately, line two in Eq. (13) has a very tiny contribution to the azimuthal velocity of the particle because of $U_\phi \sim j \ll 1$ in the suspension orbit. This proportionality relation between U_ϕ and j can be noticed from the fact that the suspension orbit in slow rotation case amounts to a critical point (see [1]) in the nonrotating case, and U_ϕ at the critical point is equal to zero, and also can be supported by subsequent calculation in Eq. (15). Therefore, all terms including U_ϕ^2 are negligible in the suspension orbit. However, in the case where it is not allowed to ignore U_ϕ such as in the initial trajectory at $r = 6M$, all the

radiation counter-drag terms, including U_ϕ^2, could contribute somewhat to the azimuthal velocity of the particle. Third, two terms in line three in Eq. (13) have overall positive definite sign, and thus line three behaves as the radiation counter drag. Since line three is proportional to the central star's angular momentum, j, the radiation counter drag of line three is due to the rotation of the central star. Also, as line three is proportional to U_ϕ^2, its contribution is negligible in the suspension orbit. Lastly, two terms of line four in Eq. (13) have overall positive definite sign, thus line four serves as the radiation counter drag. Since line four is linearly proportional to the central star's angular momentum j like the third line, the radiation counter drag of line three is also due to the rotation of the central star. However, the radiation counter drag of the fourth line acts on the test particle regardless of the velocity of the particle. Also, they are comparable to the radiation drag term of line one. Therefore, the uniform azimuthal velocity of the particle in the suspension orbit can be attributed to the terms of line four. In other words, the balance between the first line term (radiation drag) and fourth line terms (radiation counter drag) makes the particle hover around the central star with uniform azimuthal velocity. Since the radiation drag term of the first line exerts on the test particle having the specific angular momentum U_ϕ regardless of the spin (j) of the central star, this term exists even when the central star is not rotating, whereas the radiation counter-drag terms in line two through four are linearly proportional to the central star's angular momentum (j), if the central star is nonrotating, all the radiation counter-drag terms disappear. Therefore, the emergence of the radiation counter drag is attributed to the rotation of the central star. It also is of interest that there is another radiation counter-drag term proportional to the Lense-Thirring angular velocity ω and the particle's specific angular momentum square (U_ϕ^2).

Next, in order to calculate particularly the azimuthal velocity as measured by a locally static observer, we make use of normalization condition $g^{\mu\nu}U_\mu U_\nu = -1$. That is, plugging $U_r = 0$ of the conditions for the suspension orbit into the normalization condition yields

$$\left(1-\frac{2M}{r}\right)U_\phi^2 - 4j\frac{M^2}{r}U_t U_\phi + r^2\left(1-\frac{2M}{r}\right) - r^2U_t^2 = 0. \tag{14}$$

It is difficult to obtain analytically U_ϕ and U_t from the combination of Eqs. (12) and (14). Therefore, by assuming that U_ϕ^2 is negligible from our experience in the case of a nonrotating star, i.e., $U_\phi^2 \approx 0$ and neglecting terms of order higher than linear in j, we can get approximate U_ϕ and U_t, respectively, as,

$$U_\phi \approx r\left(1-\frac{2M}{r}\right)^{-1/2}\mathcal{J}(r)\left[\frac{B(\alpha)}{A(\alpha)}\right], \tag{15}$$

$$U_t \approx -2j\left(\frac{M^2}{r^3}\right)U_\phi - \left(1-\frac{2M}{r}\right)^{1/2}. \tag{16}$$

Using $\mathcal{J}(r) \sim j$ in Eq. (8), Eq. (15) indicates $U_\phi \sim j$, which is consistent with our assumption above.

The azimuthal velocity of the test particle as measured by a locally static observer is given by

$$\begin{aligned} v^{\tilde{\phi}} &= \frac{U\cdot e^{\tilde{\phi}}}{U\cdot e^{\tilde{t}}} \\ &= -\frac{1}{r}\left(1-\frac{2M}{r}\right)^{1/2}\left(\frac{U_\phi}{U_t}\right) + 2j\left(\frac{M^2}{r^2}\right)\left(1-\frac{2M}{r}\right)^{-1/2}, \end{aligned} \tag{17}$$

where $e^{\tilde{\phi}}$ and $e^{\tilde{t}}$ are tetrad associated with the locally static observer. Substitution of $\frac{U_\phi}{U_t} \approx -r(1-\frac{2M}{r})^{-1}\mathcal{J}(r)\frac{B(\alpha_0)}{A(\alpha_0)}$ obtained from Eqs. (15) and (16) into Eq. (17) yields the azimuthal velocity of the particle in the suspension orbit as measured by the locally static observer to be

$$v_{\rm att}^{\tilde{\phi}} \approx \left(1-\frac{2M}{r}\right)^{-1/2}\mathcal{J}(r)\frac{B(\alpha_0)}{A(\alpha_0)} + 2j\left(\frac{M^2}{r^2}\right)\left(1-\frac{2M}{r}\right)^{-1/2}. \tag{18}$$

The first term in Eq. (18) indicates the contribution to the azimuthal velocity of the particle in the suspension orbit due to the combination of the rotation of the star and the rotation of the radiation source which rotates with the star by being attached to the stellar surface. Since the second term in Eq. (18) is equal to the azimuthal velocity of the LNRF measured by the locally static observer, it is the contribution due to the Lense-Thirring effect (dragging of inertial frame) arising from the slow rotation of the star.

In order to obtain the coordinate radius from the center of the star to the suspension orbit, we make use of $\frac{U_r}{d\tau} = 0$ and $U_r = 0$ of the conditions characterizing the suspension orbit together with U_ϕ in Eq. (15) and U_t in Eq. (16). By inserting these into Eq. (A2) in the Appendix, that is, the r component of the equations of motion, we get

$$\left(\frac{L^\infty}{L^\infty_{\rm Edd}}\right) \approx \left(1-\frac{2M}{r}\right)^{1/2}\left[1-6j\left(\frac{M}{r}\right)\mathcal{J}(r)\frac{B(\alpha)}{A(\alpha)}\right], \tag{19}$$

and the solution of Eq. (19) is the coordinate radius $r_{\rm suspension}$ from the center of the star to the suspension orbit. As we can notice from Eq. (19), it is noteworthy that the coordinate radius r_{so} of the suspension orbit indicating the circular orbit of the particle hovering around the slowly rotating massive star depends on the luminosity parameter $(\frac{L^\infty}{L^\infty_{\rm Edd}})$ and the dimensionless angular momentum j of the star alone, and does not depend on the initial position and the initial velocity (angular momentum) of the particles. Also, since Eq. (A1) in the Appendix, that is, the t component of the equations of motion, is satisfied by Eqs. (12) and (14), the problem of overdetermining U_t and U_ϕ does

not occur. For $(\frac{L^\infty}{L^\infty_{\rm Edd}}) = 0.75$ and $j = 0.10$, Eq. (19) gives $r_{so} \simeq 4.63M$, which is similar to the value ($r_{so} \simeq 4.66M$) in the numerical integration of Sec. III. Then, plugging $r_{so} \simeq 4.63M$ and $j = 0.10$ into Eq. (18) yields $v^{\tilde{\phi}}_{\rm suspension} \simeq 0.056 = 0.044 + 0.012$, which is also very similar to the value ($v^{\tilde{\phi}} \simeq 0.056$) obtained from the numerical integration in Sec. III, where 0.044 is the contribution from Doppler shift resulting from the combination of the rotation of the star and the radiation source, and 0.012 is the contribution from the Lense-Thirring effect due to the rotation of the star. Thus, we can find that the Doppler shift due to the rotation of both the central star and the radiation source have even larger contribution to the azimuthal velocity of the test particle than Lense-Thirring effect by the rotation of the central star.

In Fig. 7, as can be seen from the comparison of the solid line [the plot of the approximate expression given by Eq. (19)] and numerical values (triangles and asterisks) obtained by the numerical integration for $j = 0.10$, above approximate Eq. (19) is valid only for $j < 0.10$. If $j = 0$ and $v = 0$, i.e., the star is nonrotating, and the radiation source does not rotate either, Eq. (19) reduces to

$$\left(\frac{L^\infty}{L^\infty_{\rm Edd}}\right) = \left(1 - \frac{2M}{r}\right)^{1/2}. \tag{20}$$

In this case, for $(\frac{L^\infty}{L^\infty_{\rm Edd}}) = 0.75$, Eq. (20) gives $r_{so} = 32M/7 \simeq 4.57M$, which is smaller than $r_{so} \simeq 4.66M$ in the slowly rotation case. Thus, the rotation of the star and the radiation source makes the suspension orbit expand outward, which is obvious from the fact that the rotation of the particles generates centrifugal force, and this force is balanced with the gravitational force and the radiation pressure.

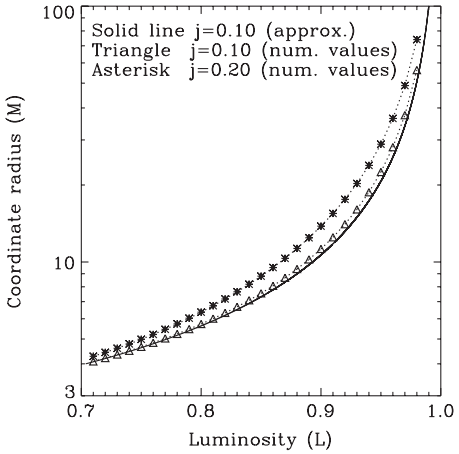

FIG. 7. shows the coordinate radius of the suspension orbit r_{so} as a function of the luminosity L for the angular momentum of the central star $j = 0.10$ and 0.20, respectively. The solid line denotes the plot of the approximate expression given by Eq. (19) for $j = 0.10$, and triangles ($j = 0.10$) and asterisks ($j = 0.20$), respectively, denote values obtained through the numerical integration.

Also, if $r_{so} = 4M$ (stellar radius) and $r_{so} = 6M$ (ISCO) in the case of $j = 0.10$, then from Eq. (19) we can get $(\frac{L^\infty}{L^\infty_{\rm Edd}}) \simeq 0.70$ and $(\frac{L^\infty}{L^\infty_{\rm Edd}}) \simeq 0.80$, respectively, so if the luminosity of the star measured at infinity lies within the range of $0.70 \leq (\frac{L^\infty}{L^\infty_{\rm Edd}}) \leq 0.80$, the suspension orbit appears in boundary layer between the stellar surface and the ISCO. Therefore, if the slowly rotating central star with radius of $R = 4M$ has luminosity of $L = 0.75$ and angular momentum of $j = 0.10$, the test particle hovers around the star with azimuthal velocity of about $0.05c$ in the boundary layer between the stellar surface and the ISCO, where the rotation direction of the particle is the same as that of the star's spin.

V. DISCUSSION

We now summarize what we have realized in the present work, which are new ingredients that have not been addressed in the previous literature. The results presented in Secs. III and IV show that there exists a suspension orbit whose location is determined by the central star's luminosity L as measured at infinity and the star's angular momentum j and is independent of the initial positions and velocities of test particles. To be more concrete, we have explored the two-dimensional motion of test particles on the equatorial plane around a slowly rotating star with the asymptotic luminosity measured at infinity in the range of $0.70 \leq (\frac{L^\infty}{L^\infty_{\rm Edd}}) \leq 1$. We found out that for the luminosity in the above range, there exist suspension orbit at which the radial velocity of the test particle vanishes and the proper time rate of change in the radial and azimuthal velocity also vanish, and the particle's azimuthal velocity U_ϕ is constant, thus the test particle hovers around the star with uniform azimuthal velocity regardless of their initial positions and velocities. And it is interesting to note that not only the radiation drag but also the radiation counter drags, which result from the central star's spin exert on the particle in the suspension orbit and the balance between the radiation drag, and the radiation counter drags make the particle hover around the star at a uniform azimuthal velocity much greater than that due to the Lense-Thirring effect (i.e., the dragging of inertial frame). Furthermore, it is noticeable that there exists another radiation counter-drag term that is proportional to the Lense-Thirring angular velocity ω.

Interestingly enough, Bini, Jantzen, and Stella [9] reported a study that happens to be akin to the motivation of our work and consistent with our results in some respects. They found the existence of the critical radius at which the test particle corotates with the geometry in the Kerr spacetime background. However, the radiation stress-energy tensor they employed is valid for only the photons in outward radial motion with zero angular momentum, and

thus is not appropriate to the applications to the accretion process onto the rotating relativistic stars like the neutron star. In the present study, on the other hand, since we employed the radiation stress-energy tensor first constructed by Miller and Lamb [3], which has no limitations whatsoever on the character of the emitted photons, our results can be applied to the accretion process onto the rotating relativistic stars.

Lastly, in the forthcoming article, we will report on our result of the study where the central luminous star is nonrotating ($j = 0$).

ACKNOWLEDGMENTS

The authors of this paper greatly appreciate the referee's suggestions, which improved the paper very much. This work was supported by the Korean Research Foundation Grant No. 2006-341-C00018. J. S. O. acknowledges the support of the BK21 program to SNU.

APPENDIX

The equations of motion (5) of a tensorial form is decomposed into each components as follows:

$$\begin{aligned}
\frac{dU_t}{d\tau} &= \frac{\sigma}{m}\left(1-\frac{2M}{r}\right)T^{t\beta}U_\beta + 2j\frac{\sigma}{m}\left(\frac{M^2}{r}\right)T^{\phi\beta}U_\beta - \frac{\sigma}{m}U_t T^{\alpha\beta}U_\alpha U_\beta \\
&= \frac{M}{3R^2}\left(\frac{L^\infty}{L^\infty_{\rm Edd}}\right)\frac{(1-2M/R)}{(1-2M/r)^2}A(\alpha_0)U_t + \frac{M}{R^2}\left(\frac{L^\infty}{L^\infty_{\rm Edd}}\right)\frac{(1-2M/R)}{(1-2M/r)}\sin^2\alpha_0 U_r \\
&\quad + \frac{M}{3R^2}\left(\frac{L^\infty}{L^\infty_{\rm Edd}}\right)\frac{(1-2M/R)}{(1-2M/r)^2}\left[2j\left(\frac{M^2}{r^3}\right)A(\alpha_0) + \left(\frac{1}{r}\right)\mathcal{J}(r)B(\alpha_0)\right]U_\phi - \frac{M}{3R^2}\left(\frac{L^\infty}{L^\infty_{\rm Edd}}\right)\frac{(1-2M/R)}{(1-2M/r)^3}A(\alpha_0)U_t^3 \\
&\quad - \frac{M}{R^2}\left(\frac{L^\infty}{L^\infty_{\rm Edd}}\right)\frac{(1-2M/R)}{(1-2M/r)^2}\left[(2\sin^2\alpha_0)U_t + \left(1-\frac{2M}{r}\right)(\cos\alpha_0\sin^2\alpha_0)U_r\right]U_t U_r \\
&\quad - \frac{M}{3R^2}\left(\frac{L^\infty}{L^\infty_{\rm Edd}}\right)\frac{(1-2M/R)}{(1-2M/r)^3}\left[4j\left(\frac{M^2}{r^3}\right)A(\alpha_0) + \left(\frac{2}{r}\right)\mathcal{J}(r)B(\alpha_0)\right]U_t^2 U_\phi \\
&\quad - \frac{M}{R^2}\left(\frac{L^\infty}{L^\infty_{\rm Edd}}\right)\frac{(1-2M/R)}{(1-2M/r)^2}\left[4j\left(\frac{M^2}{r^3}\right)(\sin^2\alpha_0) + \left(\frac{1}{2r}\right)\mathcal{J}(r)(\sin^4\alpha_0)\right]U_t U_r U_\phi,
\end{aligned} \tag{A1}$$

$$\begin{aligned}
\frac{dU_r}{d\tau} &= -\frac{1}{r} + \frac{1}{r}\left(1-\frac{2M}{r}\right)^{-2}\left(1-\frac{3M}{r}\right)U_t^2 - \frac{1}{r}\left(1-\frac{M}{r}\right)U_r^2 - 2j\left(\frac{M^2}{r^4}\right)\left(1-\frac{2M}{r}\right)^{-2}U_t U_\phi - \frac{\sigma}{m}\left(1-\frac{2M}{r}\right)^{-1}T^{r\beta}U_\beta \\
&\quad - \frac{\sigma}{m}U_r T^{\alpha\beta}U_\alpha U_\beta \\
&= -\frac{1}{r} + \frac{1}{r}\left(1-\frac{2M}{r}\right)^{-2}\left(1-\frac{3M}{r}\right)U_t^2 - \frac{1}{r}\left(1-\frac{M}{r}\right)U_r^2 - 2j\left(\frac{M^2}{r^4}\right)\left(1-\frac{2M}{r}\right)^{-2}U_t U_\phi \\
&\quad - \frac{M}{R^2}\left(\frac{L^\infty}{L^\infty_{\rm Edd}}\right)\frac{(1-2M/R)}{(1-2M/r)^3}\sin^2\alpha_0 U_t - \frac{M}{R^2}\left(\frac{L^\infty}{L^\infty_{\rm Edd}}\right)\frac{(1-2M/R)}{(1-2M/r)^2}(\cos\alpha_0\sin^2\alpha_0)U_r \\
&\quad - \frac{M}{R^2}\left(\frac{L^\infty}{L^\infty_{\rm Edd}}\right)\frac{(1-2M/R)}{(1-2M/r)^3}\left[2j\left(\frac{M^2}{r^3}\right)(\sin^2\alpha_0) + \left(\frac{1}{4r}\right)\mathcal{J}(r)(\sin^4\alpha_0)\right]U_\phi - \frac{M}{3R^2}\left(\frac{L^\infty}{L^\infty_{\rm Edd}}\right)\frac{(1-2M/R)}{(1-2M/r)^3}A(\alpha_0)U_t^2 U_r \\
&\quad - \frac{M}{R^2}\left(\frac{L^\infty}{L^\infty_{\rm Edd}}\right)\frac{(1-2M/R)}{(1-2M/r)^2}\left[(2\sin^2\alpha_0)U_t + \left(1-\frac{2M}{r}\right)(\cos\alpha_0\sin^2\alpha_0)U_r\right]U_r^2 \\
&\quad - \frac{M}{3R^2}\left(\frac{L^\infty}{L^\infty_{\rm Edd}}\right)\frac{(1-2M/R)}{(1-2M/r)^3}\left[4j\left(\frac{M^2}{r^3}\right)A(\alpha_0) + \left(\frac{2}{r}\right)\mathcal{J}(r)B(\alpha_0)\right]U_t U_r U_\phi \\
&\quad - \frac{M}{R^2}\left(\frac{L^\infty}{L^\infty_{\rm Edd}}\right)\frac{(1-2M/R)}{(1-2M/r)^2}\left[4j\left(\frac{M^2}{r^3}\right)(\sin^2\alpha_0) + \left(\frac{1}{2r}\right)\mathcal{J}(r)(\sin^4\alpha_0)\right]U_r^2 U_\phi,
\end{aligned} \tag{A2}$$

$$\frac{dU_\phi}{d\tau} = 2j\frac{\sigma}{m}\left(\frac{M^2}{r}\right)T^{t\beta}U_\beta - \frac{\sigma}{m}r^2T^{\phi\beta}U_\beta - \frac{\sigma}{m}U_\phi T^{\alpha\beta}U_\alpha U_\beta$$
$$= -\frac{M}{3R^2}\left(\frac{L^\infty}{L^\infty_{\rm Edd}}\right)\frac{(1-2M/R)}{(1-2M/r)^3}r\mathcal{J}(r)B(\alpha_0)U_t - \frac{M}{R^2}\left(\frac{L^\infty}{L^\infty_{\rm Edd}}\right)\frac{(1-2M/R)}{(1-2M/r)^2}\left(\frac{r}{4}\right)\mathcal{J}(r)(\sin^4\alpha_0)U_r$$
$$-\frac{M}{3R^2}\left(\frac{L^\infty}{L^\infty_{\rm Edd}}\right)\frac{(1-2M/R)}{(1-2M/r)^3}A(\alpha_0)U_t^2U_\phi - \frac{M}{R^2}\left(\frac{L^\infty}{L^\infty_{\rm Edd}}\right)\frac{(1-2M/R)}{(1-2M/r)^2}\left[(2\sin^2\alpha_0)U_t + \left(1-\frac{2M}{r}\right)(\cos\alpha_0\sin^2\alpha_0)U_r\right]$$
$$\times U_rU_\phi - \frac{M}{3R^2}\left(\frac{L^\infty}{L^\infty_{\rm Edd}}\right)\frac{(1-2M/R)}{(1-2M/r)^3}\left[4j\left(\frac{M^2}{r^3}\right)A(\alpha_0) + \left(\frac{2}{r}\right)\mathcal{J}(r)B(\alpha_0)\right]U_tU_\phi^2$$
$$-\frac{M}{R^2}\left(\frac{L^\infty}{L^\infty_{\rm Edd}}\right)\frac{(1-2M/R)}{(1-2M/r)^2}\left[4j\left(\frac{M^2}{r^3}\right)(\sin^2\alpha_0) + \left(\frac{1}{2r}\right)\mathcal{J}(r)(\sin^4\alpha_0)\right]U_rU_\phi^2, \tag{A3}$$

where $A(\alpha_0) = \cos^3\alpha_0 - 9\cos\alpha_0 + 8$, $B(\alpha_0) = \cos^3\alpha_0 - 3\cos\alpha_0 + 2$, and $\sin\alpha_0 = (\frac{R}{r})(\frac{1-2M/r}{1-2M/R})^{1/2}$.

[1] M. A. Abramowicz, G. F. R. Ellis, and A. Lanza, Astrophys. J. **361**, 470 (1990).
[2] M. Coleman Miller and F. K. Lamb, Astrophys. J. **413**, L43 (1993).
[3] M. Coleman Miller and F. K. Lamb, Astrophys. J. **470**, 1033 (1996).
[4] R. Kerr, Phys. Rev. Lett. **11**, 237 (1963).
[5] J. Lense and H. Thirring, Phys. Zh. **19**, 156 (1918).
[6] J. M. Bardeen, Astrophys. J. **162**, 71 (1970).
[7] J. M. Bardeen, W. H. Press, and S. A. Teukolsky, Astrophys. J. **178**, 347 (1972).
[8] F. K. Lamb and M. Coleman Miller, Astrophys. J. **439**, 828 (1995).
[9] D. Bini, R. T Jantzen, and L. Stella, Classical Quantum Gravity **26**, 055009 (2009).